Journal of Power Sources 196 (2011) 814–819

Contents lists available at ScienceDirect

Journal of Power Sources

journal homepage: www.elsevier.com/locate/jpowsour

Short communication

Electrochemical insertion/deinsertion of sodium on NaV_6O_{15} nanorods as cathode material of rechargeable sodium-based batteries

Haimei Liu [a,*], Haoshen Zhou [b], Lipeng Chen [a], Zhanfeng Tang [a], Wensheng Yang [a,*]

[a] State Key Laboratory of Chemical Resource Engineering, Beijing University of Chemical Technology, Beijing 100029, China
[b] Institute of Energy Technology, National Institute of Advanced Industrial Science and Technology (AIST), AIST Tsukuba Center 2, Umezono 1-1-1, Tsukuba, Ibaraki 305-8568, Japan

ARTICLE INFO

Article history:
Received 1 June 2010
Received in revised form 14 July 2010
Accepted 21 July 2010
Available online 4 August 2010

Keywords:
Rechargeable sodium battery
Cathode materials
NaV_6O_{15}
Electrochemical performance

ABSTRACT

A well defined nano-structured material, NaV_6O_{15} nanorods, was synthesized by a facile low temperature hydrothermal method. It can perform well as the cathode material of rechargeable sodium batteries. It was found that the NaV_6O_{15} nanorods exhibited stable sodium-ion insertion/deinsertion reversibility and delivered 142 mAh g^{-1} sodium ions when worked at a current density of 0.02 A g^{-1}. In galvanostatic cycling test, a specific discharge capacity of around 75 mAh g^{-1} could be obtained after 30 cycles under 0.05 A g^{-1} current density. Concerned to its good electrochemical performance for reversible delivery of sodium ions, it is thus expected that NaV_6O_{15} may be used as cathode material for rechargeable sodium batteries with highly environmental friendship and low cost.

1. Introduction

Rechargeable lithium-ion battery, due to its excellent electrochemical properties, has becoming an important energy storage system in the modern society. Accordingly, much effort has been made to study the lithium-ion battery in recent years [1–6]. However, the further development on rechargeable lithium-ion battery is still facing a series challenge which is arising from the cathode materials. First, the most dominant cathode materials of today's rechargeable Li-ion batteries are lithium transition metal oxides, such as $LiCoO_2$, $LiNiO_2$, $LiMn_2O_4$, *etc.*, the limited ores resources of these materials make them expensive. In the future, if the real electric vehicles (EVs) or hybrid EVs (HEVs) generation comes, it will put considerable strain on resources and hence cost effectiveness, therefore limit its practical application. Second, safety issue is another big concern in terms of large-scale applications of battery, especially in EVs and HEVs [7–9]. The usage of electrolyte with high decomposition potential which is strictly necessary for presently employed cathode materials, brings about a big risk of which can cause severe thermal runaway reactions leading to either fire or explosion of the cell in the case of improper use such as overcharging or short-circuiting. Is there any solution to keep away from these risks in future's battery system?

Sodium-based batteries seem to be a good choice when consideration of above-mentioned issues, since it has been attracted considerable attentions in past several years [10–15]. Apparently, sodium-based batteries have some significant merits, such as the low cost of the raw materials, higher environmental friendship [10–13], moreover, since the redox potential of Na (−2.71 V *vs.* NHE) is not as negative as that of Li (−3.05 V *vs.* NHE), the output voltage of the cell based on the negative electrode of Na metal or alloys should be lower compared with that of Li, therefore even though the electrolyte solution possessing a similar decomposition potential as that of presently used in lithium-ion batteries, it will become more safe, of course, at the expense of the high energy density of the cell. Actually, in recent years, some promising cathode materials for rechargeable sodium battery have been well studied, e.g., MF_3 (M = Fe, V, Mn, Co and Ti), Cu_2S, $NaV_{1-x}Cr_xPO_4F$, Na_2FePO_4F, *etc.*, [10–13]. However, all of these materials containing corrosive fluorine or sulfur, of which are relatively less environmentally friendly. Moreover, fluorides and sulfate are basically unstable in moisture atmosphere [10], which easily leads to decomposition when the cell is improper used by over-charging or over-discharging. At the same time, the fluoride is usually prepared in high-pressure fluorination with F_2 gas, or solid-state reaction under inter-conditions and high temperature, complex formation reaction by precipitation with HF acid, *etc.*, thus some unknown fluorine species is always residual on the sample surface, it is therefore induced some unexpected reactions during the cell operation. Hence, there has still a big space to develop more suitable candidate cathode materials for rechargeable sodium-based batteries.

* Corresponding authors. Tel.: +86 10 6443 5271; fax: +86 10 6442 5385.
E-mail addresses: liuhm@mail.buct.edu.cn (H. Liu), yangws@mail.buct.edu.cn (W. Yang).

0378-7753/$ – see front matter © 2010 Elsevier B.V. All rights reserved.
doi:10.1016/j.jpowsour.2010.07.062

The ionic volume of sodium ions is almost twice of that of lithium ions, only those of materials possessing two-dimensional layered structures or three-dimension with corner sharing matrix, and or crystal structure forming suitable large-size tunnels can reversibly accommodate sodium ions. Recently, a number of oxide materials of potential interest were studied as cathode materials of sodium battery, for instance, Na_xCoO_2, Na_xMnO_2, $Na_{0.44}MnO_2$, and Fe_3O_4 [12–15]. However, the poor reversibility of intercalation and deintercalation of sodium ions on aforementioned materials and the lower reversible capacity make them far from the satisfied target performance for sodium battery.

More recently, we reported a cathode material of NaV_6O_{15} nanorods [16], of which was successfully applied for secondary lithium battery and exhibited stable lithium-ion insertion/deinsertion reversibility and delivered as high as 328 mAh g^{-1} lithium when cycled at a current density of 0.02 A g^{-1}. Moreover, in early work it was demonstrated that the bulk material of NaV_6O_{15} ($Na_{0.33}V_2O_5$) was able to insert and extract sodium reversibly in electrochemical cells, and revealed a maximum amount of around 1.6Na were inserted into the host electrode of $Na_{0.33}V_2O_5$ [17–19]. On the other hand, it is generally accepted that the nanoscaled materials can provide high specific surface area, short ion diffuse pathway, all of which are beneficial to the battery performance [20–22]. In this paper, the electrochemical performances of NaV_6O_{15} nanorods material for reversible accommodation of sodium ions were investigated.

2. Experiment

The NaV_6O_{15} nanorod was synthesized by a facile hydrothermal method, typically a V_2O_5 powder (0.364 g) dispersed in 30 mL distilled water was mixed with 5 mL 30% H_2O_2 and NaCl (1.5 g, 99.5%) under vigorous stirring at room temperature and kept for 2 h, a transparent orange solution was thus obtained. The resultant solution was then transferred to a 40 mL autoclave and kept in an oven at 205 °C for 4 days, in the same way as elsewhere described [16]. The freshly prepared precursor was finally post-treated in air at 500 °C for 2 h, because this treatment condition gave the optimal performance of NaV_6O_{15} nanorods in reversible delivery of lithium ions [16]. Powder X-ray diffraction (XRD) data for the synthesized materials were collected with a Bruker D8 Advanced diffractometer using CuKα (λ = 1.5406 Å) radiation. Scanning electronic microscopy (SEM) and Transmission Electron Microscopy (TEM) images were taken on LEO Gemini Supra 35 and Hitachi 800 instruments, respectively.

The electrochemical performance of the synthesized NaV_6O_{15} sample was measured with a beaker-type two-electrode cell. The working electrode (WE) was composed of 80% NaV_6O_{15}, 15% acetylene black (AB), and 5% polytetrafluoroethylene (PTFE) binder by weight. The above mixtures were spread and pressed onto a titanium mesh (100 mesh) which served as a current collector. The sodium metal was spreaded and pressed onto a similar titanium mesh as the reference electrode (RE) and counter electrode (CE). The electrolyte was 1 M $NaClO_4$ in ethyl carbonate (EC) and diethyl carbonate (DEC) (EC/DEC = 1:1, v/v). For *ex situ* XRD, SEM measurement, the NaV_6O_{15} electrode after electrochemical cycling was carefully disassembled and washed by EC pure solution in Ar-filled glove box, and dried in a vacuum oven.

3. Results and discussion

The as-synthesized NaV_6O_{15} nanorods were characterized as shown in Fig. 1. The SEM image (Fig. 1a) reveals that these NaV_6O_{15} nanorods are around 100–200 nm in width and several micrometers in length, XRD patterns (Fig. 1b) demonstrate the highly crystallized structure and all the diffraction peaks can be assigned

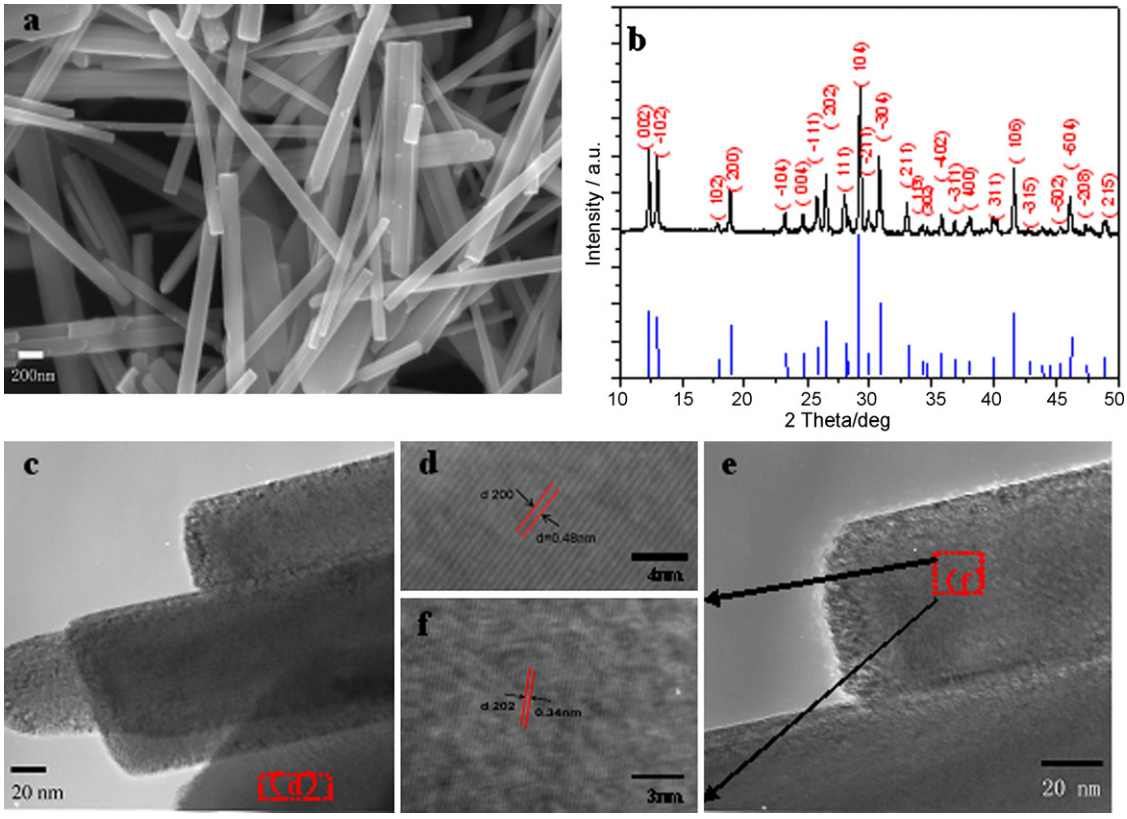

Fig. 1. Characterizations of as-prepared NaV_6O_{15} nanorods, (a) SEM image, (b) XRD patterns, (c–f) TEM and HRTEM images.

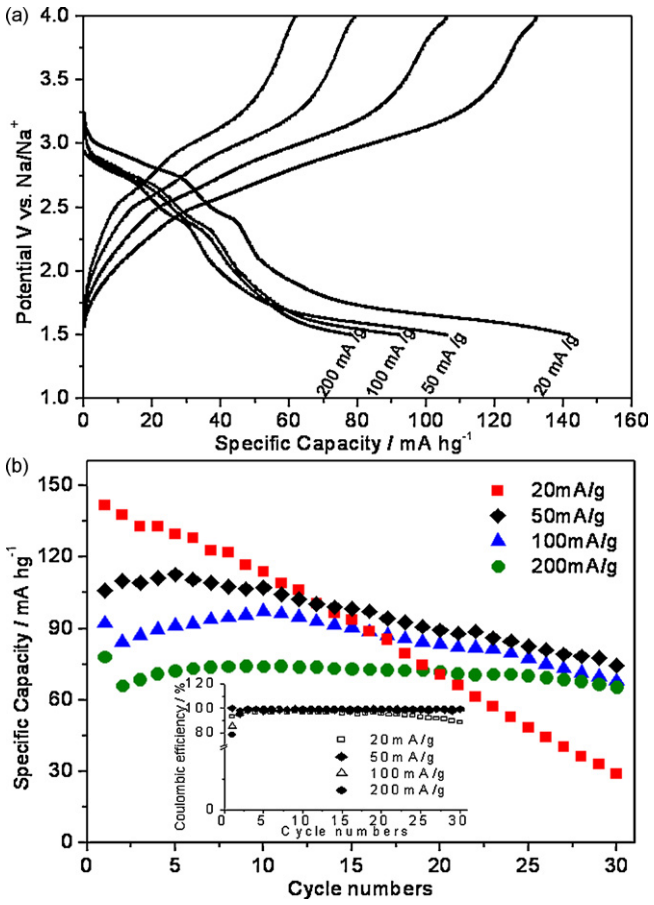

Fig. 2. (a) The first cycle profiles of charge–discharge measurement, (b) cycle performance and coulombic efficiency (inset) of NaV_6O_{15} nanorods at various current densities. All the cells were worked within the potential window of 4.0–1.5 V (*vs.* Na/Na^+) from 1 M $NaClO_4$ in ethyl carbonate (EC) and diethyl carbonate (DEC) (EC/DEC = 1:1, v/v).

well to the monoclinic layered NaV_6O_{15} phase (space group: *A2/m (12)*, JCPDS No: 24-1155), this result is in a good agreement with that of previously reported [16], implying a good reproducibility of the present method for preparation of NaV_6O_{15} nanorods. Fig. 1c–f displays the TEM and HRTEM images. As clearly seen from Fig. 1d that is come from the dotted line area of Fig. 1c, the lattice fringe parallel to the longitudinal direction with 0.48 nm interplanar distance can be observed, which is in a good match with the *d*-spacing of (2 0 0) planes of monoclinic layered NaV_6O_{15} (JCPDS No.: 24-1155), indicating that the width direction of the nanorods is corresponding to the *a* axis of the crystal structure. This argument is further supported by the lattice fringe in Fig. 1f which is derived from the marked square area in Fig. 1e. The lattice fringe with 0.34 nm inter-planar distance, of which can be indexed to the (2 0 2) planes, is almost perpendicular to the preferred orientation of the nanorods, thereby we can deduce that the preferred orientation of the nanorods is *c* direction, Thus, the *b* axis is the thickness direction of the nanorods with around several tens nanometers, this nano-sized dimension maybe facilitate the Na^+ transposition, it will be discussed later.

Fig. 2a gives the first cycles of typical charge/discharge profiles of the NaV_6O_{15} nanorods. The cell was worked between 1.5 and 4.0 V *vs.* Na/Na^+ at various current densities. It is amazing to notice that, at lower current density of 20 mA g^{-1}, an initial discharge capacity of 142 mAh g^{-1} was demonstrated, one of the highest capacities reported to date concerned the Na^+ insertion materials [10–15]. With increasing of the current densities to 50, 100 and 200 mA g^{-1}, the discharge capacities are 106, 92, and 78 mAh g^{-1}, respectively, the decreasing of the capacities demonstrate somewhat kinetic limitations at the higher current flows. At a lower current density of 20 mA g^{-1}, there are two apparent voltage plateaus at 2.7 and 2.3 V, corresponding 0.5 and 1Na^+ were inserted into the host NaV_6O_{15}. It was reported that the diffusion coefficient of sodium ions in NaV_6O_{15} ($Na_{0.33}V_2O_5$) bulk materials was one or two magnitude lower than that of the lithium ions [17–19], therefore, the rate capacity of Li^+ insertion/deinsertion was better than that of the Na^+, for instance, when current density was increased from 100 μA to 1 mA during the Li^+ test, the inserted amount of Li^+ was only decreased from about 1.55Li to 1.15Li [19], whereas as for the Na^+, when current density was increased from 50 to 500 μA, the inserted amount of sodium was quickly decreased from 1.3Na to 0.26Na in bulk material, only 20% of the capacity could be retained [17]. However, it is worthwhile to be noted that the rate capacity of the present NaV_6O_{15} nanorods is somewhat better than that of the bulk material for Na^+ insertion/deinsertion, of which as displayed in Fig. 2a on nanorods electrodes, nearly 55% of the discharge capacity was maintained when current density increased from 20 to 200 mA g^{-1}.

The characteristic feature in crystallographic of NaV_6O_{15} is that it is formed by $(V_2O_5)_x$ framework, of which was constructed by VO_5 pyramid and VO_6 octahedra with three crystallographically distinct vanadium sites, labeled as V_1, V_2 and V_3. The framework has tunnels along *b* axis, and Na cations are aligned in these tunnels [23,24]. In our previous work, it was found that not only the Li^+ can be reversibly insert and deinsert into/out of this tunnels along *b* direction, but also a partial of Na^+ in crystallographic can be substituted, therefore induced a capacity increasing phenomena in the initial stage, and further confirmed by the XPS spectra [16]. In this work, Fig. 2a tells us that Na^+ can also be reversibly intercalated and deintercalated upon the NaV_6O_{15} nanorods material, and most probably in the same manner as that of Li^+, namely, the *b* direction is the main path for Na^+ diffusion. As already mentioned earlier, the thickness direction of the present NaV_6O_{15} nanorods is exactly the *b* orientation with several tens nanometers in size (Fig. 1), therefore the rate performance was improved (Fig. 2a).

To further get some insights on long-term stability of NaV_6O_{15} nanorods, the cycling performance was investigated in a galvanostatic mode at various current densities as shown in Fig. 2b. The capacity retention is not good at lower current density of 20 mA g^{-1}, because only about 22% of the initial capacity is retained after 30 cycles. However, when the current densities are increased to 50, 100 and 200 mA g^{-1}, the capacities decay is much suppressed and retained 71, 74 and 85% after 30 cycles, respectively. For instance, at 50 mA g^{-1}, after 30 cycles, a capacity of 75 mAh g^{-1} can be obtained, it is still on the high class of discharge capacity as well as capacity retention on sodium-ion insertion materials [10–15,25], for example, at a very low current density of C/10, a rod-like $Na_{0.44}MnO_2$ displayed an initial capacity of 82 mAh g^{-1} for accommodation of Na^+, and decayed to around 65 mAh g^{-1} after 30 cycles [14]. Note also that although the capacity decays are observed at all tested current densities (Fig. 2b), the coulombic efficiencies displayed in Fig. 2b (inset) are in general maintained at around 100%, except of at 20 mA g^{-1} together with all of the first cycles. The deviation of coulombic efficiency from 100% under 20 mA g^{-1} may be explained by: firstly, the full reduction of NaV_6O_{15} to 1.5 V under a quite small current density induces that it is difficult to complete extraction of Na^+ at consequent charge process; secondly, the extensive discharge depth may bring about a collapse of the crystallographic structure of the material.

The above argument is strongly supported by the cycling life test with controlling of cut-off potential window at different current rates. Fig. 3a exhibits the cycling performance within the potential

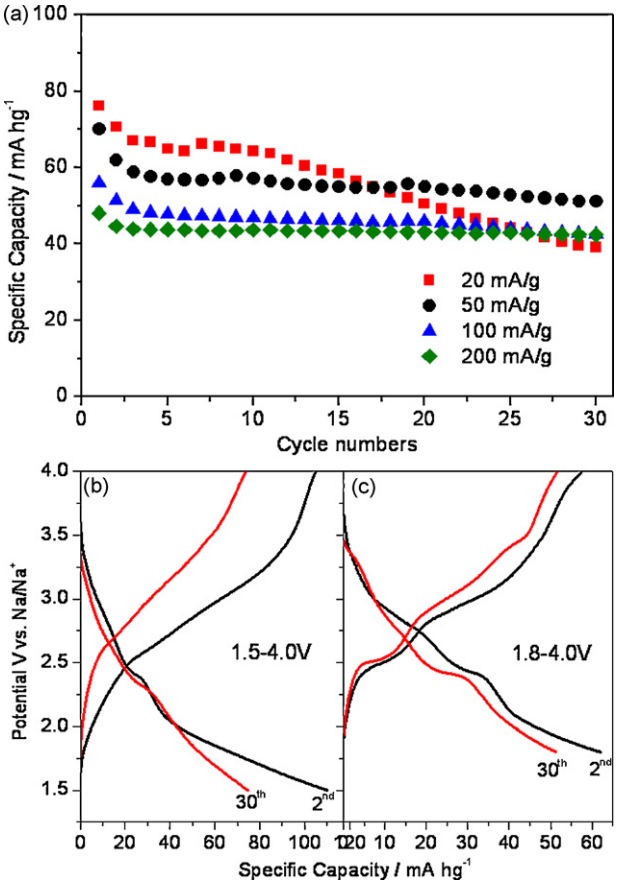

Fig. 3. (a) Cycle performance at various current densities in the potential window of 4.0–1.8 V (*vs.* Na/Na^+); (b) charge–discharge curves of second and thirtieth cycles at 50 mA g^{-1} within 4.0–1.5 V potential window; (c) within 4.0–1.8 V *vs.* Na/Na^+.

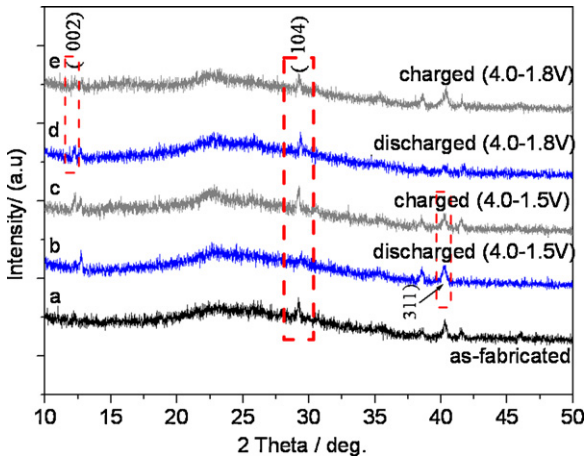

Fig. 4. XRD patterns of the electrode made of NaV_6O_{15} nanorods, curve a: as-fabricated; b: discharged to 1.5 V after the 5th cycle; c: charged to 4.0 V during the 5th cycle within 1.5–4.0 V; d: discharged to 1.8 V after the 5th cycle; e: charged to 4.0 V during the 5th cycle within 1.8–4.0 V.

window of 4.0–1.8 V *vs.* Na/Na^+. It is noticeable that the cycling performance at all current densities are greatly improved within this work window, even at the 20 mA g^{-1}. Thereby the capacity decays in Fig. 2b can be explained by mainly the deep discharge process, and consequence of a destroy on the crystal structure as well as the diffusion tunnels of sodium ions. Fig. 3b and c gives a comparison of charge–discharge profiles at second and thirtieth cycles, within 4.0–1.5 and 4.0–1.8 V *vs.* Na/Na^+. Within 4.0–1.5 V (Fig. 3b), the discharge plateaus become indistinct even from the second cycle, and furthermore, there are no any visible patent plateaus in the charge profiles, all of which indicate a diffusion behavior of Na^+ in an amorphous phase of NaV_6O_{15}.

On the contrary, when cycled within the potential window of 4.0–1.8 V (Fig. 3c), an obvious discharge plateaus at 2.4 V together with a charge plateaus at 2.55 V can be observed till to the 30 cycles, implying that Na^+ was inserted and deinserted upon a phase-to-phase transformation behavior in this case. Furthermore, the polarization and internal-resistance are not increased as much as that of in the 4.0–1.5 V (Fig. 3b), all of the above evidences make our earlier explanation on capacity decay in Fig. 2b are not unreasonable.

In order to demonstrate the changes on the crystallographic structure of the NaV_6O_{15} nanorods before and after electrochemical measurements, an *ex situ* XRD was employed on the cathodes material recovered from the cell at selected potential window. Fig. 4 displays the XRD patterns of the electrode at various selected conditions. Curve a in Fig. 4 is the as-fabricated electrode, the strongest pattern of (1 0 4) as seen in the powder sample (Fig. 1b) is clearly observed. However, when discharged to 1.5 V after 5 cycles, this pattern becomes weak and even indistinct (curve b), implying that the ordered crystal structure is somewhat destroyed and becomes amorphous phase, in a good agreement with our aforementioned argument and noticed result (Fig. 3b). When charged to 4.0 V again, it can be recovered to some extent (curve c). The XRD patterns of the electrode discharged to 1.8 V and subsequently charged to 4.0 V (curves d and e) are nearly same as those of before electrochemical measurement (curve a), suggesting that in this potential window, the sodium ions can be smoothly inserted and deinserted without obvious influence on the crystal structure of the electrode material, thereby the cycling stability is improved in this case (Fig. 3a). Note also that, (3 1 1) peak of 1.5 V discharged state (Fig. 4b) is stronger than that of 4.0 V charged state (Fig. 4c), and (0 0 2) peak of 1.8 V discharged state (Fig. 4d) is stronger than that of 4.0 V charged state (Fig. 4e), implying that the fine crystallographic structure of the nanorods on fully charged state and discharged state is somewhat different. However, in a long-range ordered structure, the XRD patterns on charged and discharged state (Fig. 4b–f) were still maintained as those of the freshly crystallized NaV_6O_{15} (Fig. 4a).

Finally, we may wonder whether the nanorods morphology before and after electrochemical test was maintained or not, Fig. 5 reveals the SEM micrographs of the nanorods electrode in a controlled potential window of 1.5–4.0 V at different cycling stages. Before the current is applied (panels a and b), the NaV_6O_{15} nanorods is just observed being mixed with particular conductive additive (AB), and the surface of the nanorods is flat and clear, quite similar with that of the powder sample (Fig. 1a). When discharged to 1.5 V (panels c and d) accompanied with the insertion of Na^+ into the host nanorods, it is noticeable that the nanorods is somewhat exfoliated and broken. It should be mentioned that such an exfoliation on the positive electrode materials during the cell operation in lithium-based batteries was seldom reported, nor mentioned by other sodium inserted materials [10–15,17–19,25], only once documented that a similar exfoliation of a cathode material of $Cu_{2.33}V_4O_{11}$ had ever been noticed during the Li^+ insertion, its layered structure was a key factor caused that [26], therefore we may tentatively propose that the exfoliation on NaV_6O_{15} nanorods electrode upon the Na^+ intercalation may also be induced by its unique layered crystal structure and 1D orientation growth, as well as the relatively large ionic volume of the inserted sodium ions. However, in the subsequent charge process, generally, the nanorods morphology can be recovered (panel e), except that the surface of the rods become rough (panel f). Note that the crystallographic structure is also recovered, as confirmed by the XRD patterns (Fig. 4, curve c).

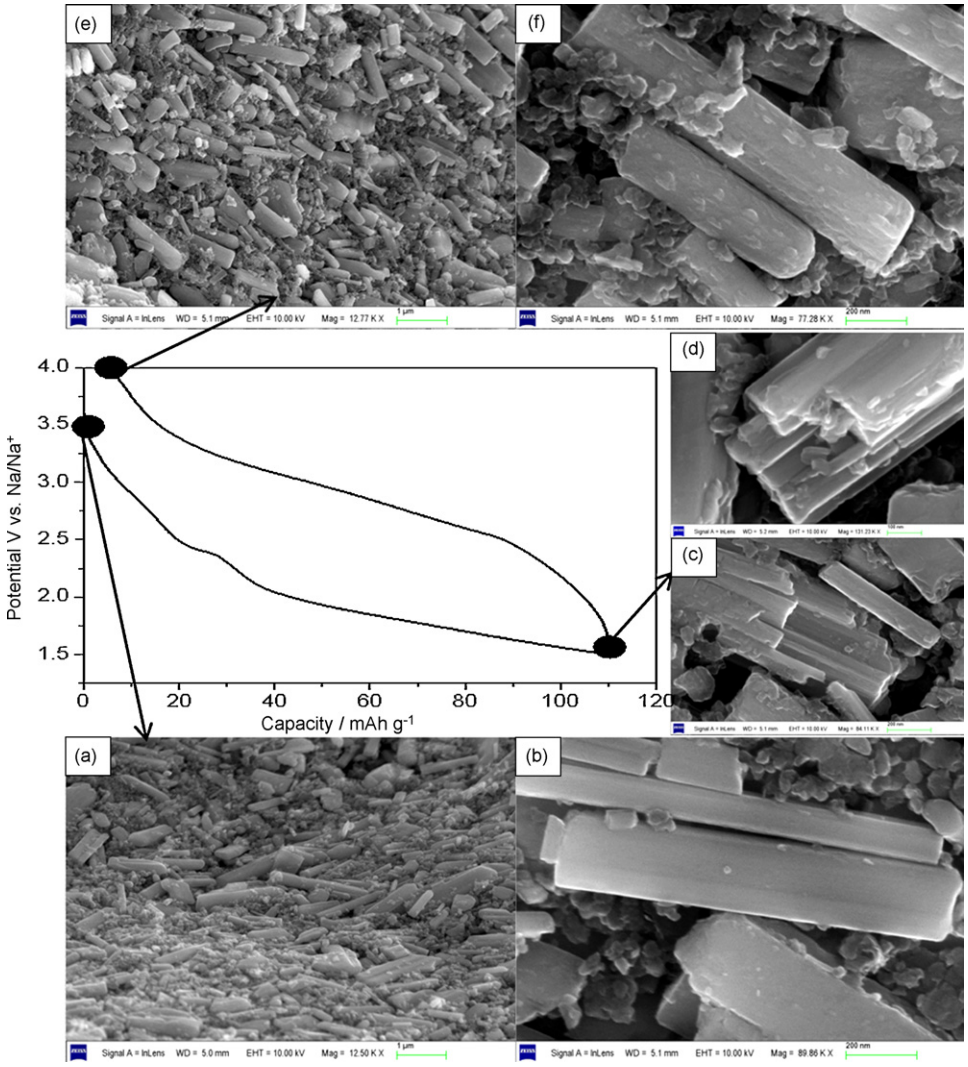

Fig. 5. *Ex situ* SEM observations of a NaV_6O_{15} nanorods electrode, (a and b) before electrochemical measurement; (c and d) discharged to 1.5 V; (e and f) charged to 4.0 V *vs.* Na/Na^+.

The electrochemical reduction of the NaV_6O_{15} cathodic material involves a charge transfer, of which is accompanied by a V^{5+}/V^{4+} redox reaction, at the same time, a Na^+ ion is transported from electrolyte solution into the crystal framework to neutralize the charge. The ionic volume of sodium ions is almost twice of that of lithium ions and the diffusion coefficient of sodium ions in NaV_6O_{15} ($Na_{0.33}V_2O_5$) is one or two magnitude lower than that of the lithium ions, therefore it is easy to understand that the accommodation ability of sodium ions on NaV_6O_{15} electrode is smaller than that of lithium ions [16–19]. A bulk material of NaV_6O_{15} ($Na_{0.33}V_2O_5$) prepared by a sol–gel process was once recorded that a maximum amount of $1.6Na^+$ could be inserted, corresponding to a maximum discharge capacity of 225 mAh g^{-1} [17,19]. In this work, the highest capacity of 142 mAh g^{-1} can be demonstrated at the lower current density. Note that although the present nanorods electrode has not contributed to improve its discharge capacity, with respect to its bulk material [17–19], it is still one of the highest capacity value of the positive electrode concerned the Na^+ insertion materials [10–15,25]. Moreover, the rate capacity of the NaV_6O_{15} nanorods is improved, most probably benefited from its smaller size along the Na^+ diffusion pathway in the *b* direction of the nanorods. Of course, there are still much work should be done in the future, for instance, how to improve the stability of the material with a higher capacity, the detailed mechanism of Na^+ diffusion and electrical conductivity, *etc*., and it is really on the going way now.

4. Conclusion

In summary, NaV_6O_{15} nanorods was first time confirmed that it has the capability to reversibly delivery of Na^+, an initial discharge capacity of 142 mAh g^{-1} could be reached at a lower current density. Furthermore, it is demonstrated that the rate performance of the nanorods NaV_6O_{15} is better than that of bulk material. By carefully controlling of the cut-off potential window and current rate, the specific capacity and reversible stability might be improved well. The crystalline structure and morphology of the nanorods could be retained stable during the electrochemical cycling. As a novel inexpensive green cathode material for rechargeable sodium-ion battery, further work is needed to optimize its work condition.

Acknowledgements

This work was financially supported by the National Nature Science Foundation of China (No. 50952008) and the 111 Project (No. B07004).

References

[1] J.M. Tarascon, M. Armand, Nature 414 (2001) 359.
[2] M.S. Whittingham, Chem. Rev. 104 (2004) 4271.
[3] M. Armand, J.M. Tarascon, Nature 451 (2008) 652.
[4] (a) N.H. Zhao, G.J. Wang, Y. Huang, B. Wang, B.D. Yao, Y.P. Wu, Chem. Mater. 20 (2008) 2612;
(b) Y.G. Wang, W. Wu, L. Cheng, P. He, C.X. Wang, Y.Y. Xia, Adv. Mater. 20 (2008) 2166.
[5] (a) X. Zhu, Z. Guo, P. Zhang, G. Du, R. Zeng, Z. Chen, H. Liu, ChemPhysChem 10 (2009) 3101;
(b) E. Hosono, T. Kuto, I. Honma, H. Matsuda, H.S. Zhou, Nano Lett. 9 (2009) 1045.
[6] (a) M. Yoshio, H. Wang, K. Fukuda, T. Umeno, T. Abe, Z. Ogumi, J. Mater. Chem. 14 (2004) 1754;
(b) H.M. Liu, Y.G. Wang, K.X. Wang, E. Hosono, H.S. Zhou, J. Mater. Chem. 19 (2009) 2835.
[7] P. Arora, Z. Zhang, Chem. Rev. 104 (2004) 4419.
[8] K. Xu, Chem. Rev. 104 (2004) 4303.
[9] P. Novák, K. Müller, K.S.V. Santhanam, O. Haas, Chem. Rev. 97 (1997) 207.
[10] I.D. Gocheva, M. Nishijima, T. Doi, S. Okada, J. Yamaki, T. Nishida, J. Power Sources 187 (2009) 247.
[11] B.L. Ellis, W.R.M. Makahnouk, Y. Makinura, K. Toghill, L.F. Nazar, Nat. Mater. 6 (2007) 749.
[12] H. Zhuo, X. Wang, A. Tang, Z. Liu, S. Gamboa, P.J. Sebastian, J. Power Sources 160 (2006) 698.
[13] S. Komaba, T. Mikumo, A. Ogata, Electrochem. Commun. 10 (2008) 1276.
[14] F. Sauvage, L. Laffont, J.M. Tarascon, E. Baudrin, Inorg. Chem. 46 (2007) 3289.
[15] T. Shiratsuchi, S. Okada, J. Yamaki, T. Nishida, J. Power Sources 159 (2006) 268.
[16] H.M. Liu, Y.G. Wang, L. Li, K.X. Wang, E. Hosono, H.S. Zhou, J. Mater. Chem. 19 (2009) 7885.
[17] S. Bach, N. Baffier, J.P.P. Ramos, R. Messina, Solid State Ionics 37 (1989) 41.
[18] K. West, B.Z. Christiansen, T. Jacobsen, S. Skaarup, Solid State Ionics 28–30 (1988) 1128.
[19] J.P.P. Ramos, R. Messina, S. Bach, N. Baffier, Solid State Ionics 41–41 (1990) 970.
[20] A.S. Aricò, P. Bruce, B. Scrosati, J.M. Tarascon, W.V. Schalkwijk, Nat. Mater. 4 (2005) 366.
[21] J. Chen, F. Cheng, Acc. Chem. Res. 42 (2009) 713.
[22] Y. Wang, G. Cao, Adv. Mater. 20 (2008) 2251.
[23] T. Yamauchi, Y. Ueda, N. Môri, Phys. Rev. Lett. 89 (2002) 057002.
[24] C. Presura, M. Popinciuc, P.H.M. Loosdrecht, D. Van der Marel, M. Mostovoy, Phys. Rev. Lett. 90 (2003) 026402.
[25] M. Nishijima, I.D. Gocheva, S. Okada, T. Doi, J. Yamaki, T. Nishida, J. Power Sources 190 (2009) 558.
[26] M. Morcrette, P. Rozier, L. Dupont, E. Mugnier, L. Sammier, J. Galy, J.M. Tarascon, Nat. Mater. 21 (2003) 755.